Supporting Information for

The Nature of Excimer Formation in Crystalline Pyrene Nanoparticles

Ryan D. Pensack,[1] Rachel J. Ashmore,[2] Angela L. Paoletta,[1] Gregory D. Scholes[1]

[1] Department of Chemistry, Princeton University, Princeton, New Jersey 08544, United States
[2] Department of Chemistry, Millersville University, Millersville, Pennsylvania 17551, United States

Table of Contents:

Section S1: Additional details of sample preparation

In order to promote strong excitonic interactions between pyrene chromophores in the nanoparticles and ensure reproducibility, we found it necessary to develop an adapted form of flash precipitation. To promote strong excitonic interactions between chromophores, we found it necessary to inject a cooled (5 °C) pyrene/THF solution at a pyrene concentration of 2 mM into 5 mL of a vigorously stirring and cooled (5 °C) 0.1 mg/mL aqueous polyvinyl solution. Immediately following the injection, the resultant aqueous nanoparticle suspension was then stored at 5 °C for a period of two hours.

Figure S1.1 shows the effect of using a polymer additive in either a room temperature or cooled (5 °C) aqueous solution.

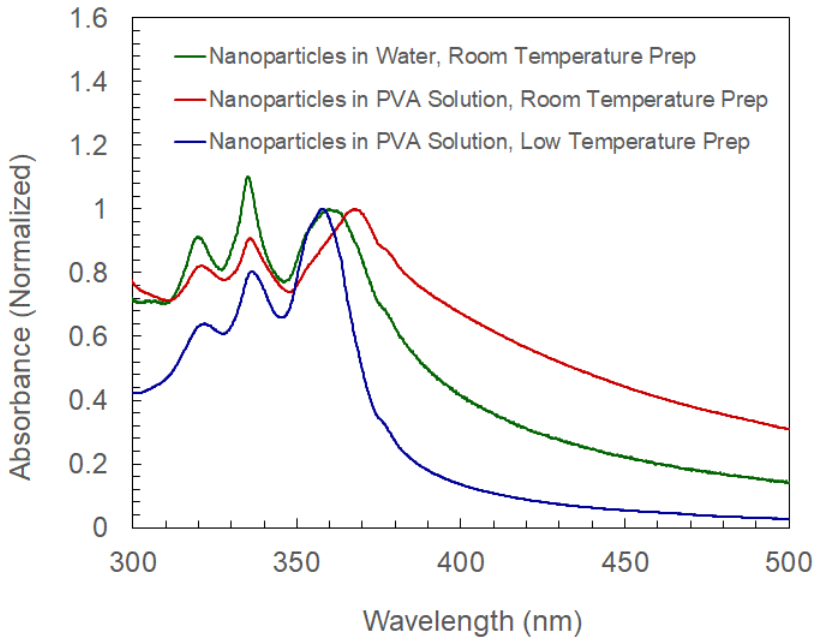

Figure S1.1. Absorption spectra of pyrene nanoparticles prepared as aqueous suspensions at room temperature, as suspensions in an aqueous polyvinyl alcohol solution at room temperature, and as suspensions in an aqueous polyvinyl alcohol solution at low (5°C) temperature.

Using polyvinyl alcohol as a polymer additive and a cooled solution (5 °C) seemed the best able to suppress monomer absorption features and promote excitonically-redshifted features. On the basis of these results, we chose to work with a polymer additive in a cooled (5 °C) aqueous solution.

Figure S1.2 shows the effect of varying the chemical structure of the polymer additive.

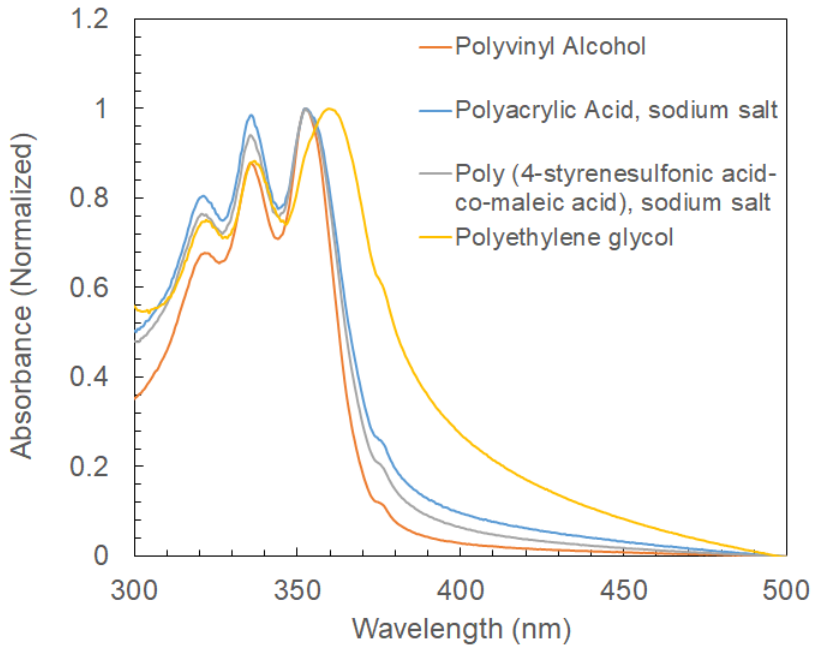

Figure S1.2. Absorption spectra of pyrene nanoparticles prepared as a function of the polymer added to the aqueous solution. These particular samples were prepared by injecting 0.1 mL of 2 mM pyrene into 10 mL of rapidly stirring 0.1 mg/mL polymer:water solution, and subsequently storing the nanoparticle suspensions at 5 ^{o}C for a period of 2 hrs.

Out of the four polymers investigated, polyvinyl alcohol was best able to suppress monomer absorption features and promote excitonically-redshifted features. On the basis of these results, we chose polyvinyl alcohol as the polymer additive.

Figure S1.3 shows the effect of varying the concentration of polyvinyl alcohol in the aqueous solution.

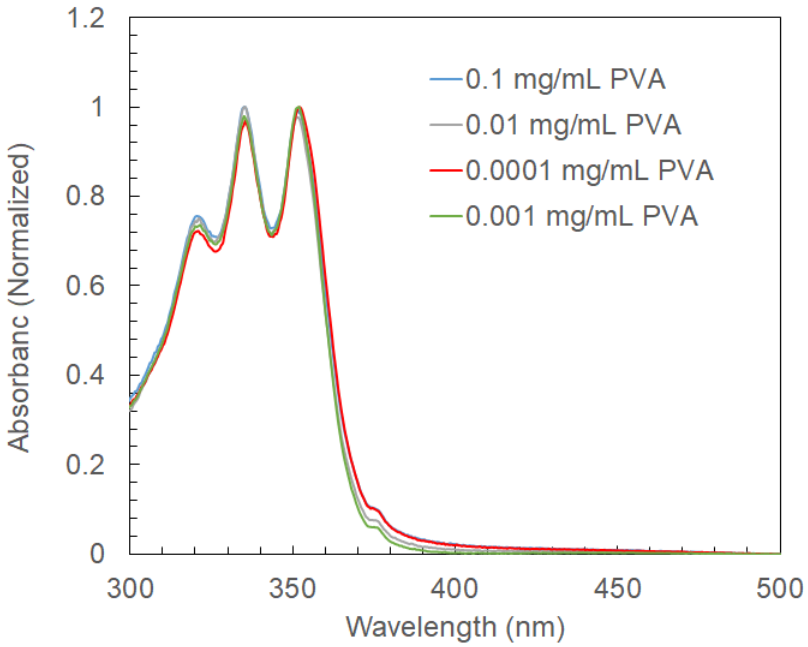

Figure S1.3. Absorption spectra of pyrene nanoparticles prepared as a function of the concentration of the PVA:water solution. These particular samples were prepared by injecting 0.2 mL of 1 mM pyrene into 10 mL of rapidly stirring PVA:water solution, and subsequently storing the nanoparticle suspensions at 5 ^{o}C for a period of 2 hrs.

Polymer additive concentration seemed to have very little influence on the suppression of the monomer absorption features and promotion of excitonically-redshifted features. On the basis of these results, we chose a concentration of 0.1 mg/mL for the aqueous polyvinyl alcohol solution. An additional factor in this decision was that 0.1 mg/mL aqueous polyvinyl alcohol solutions were previously shown to promote complete crystallization of nanoparticles of the organic semiconductor TIPS-pentacene.[S1]

Figure S1.4 shows the effect of using either a room temperature or cooled (5 °C) pyrene / THF injection solution.

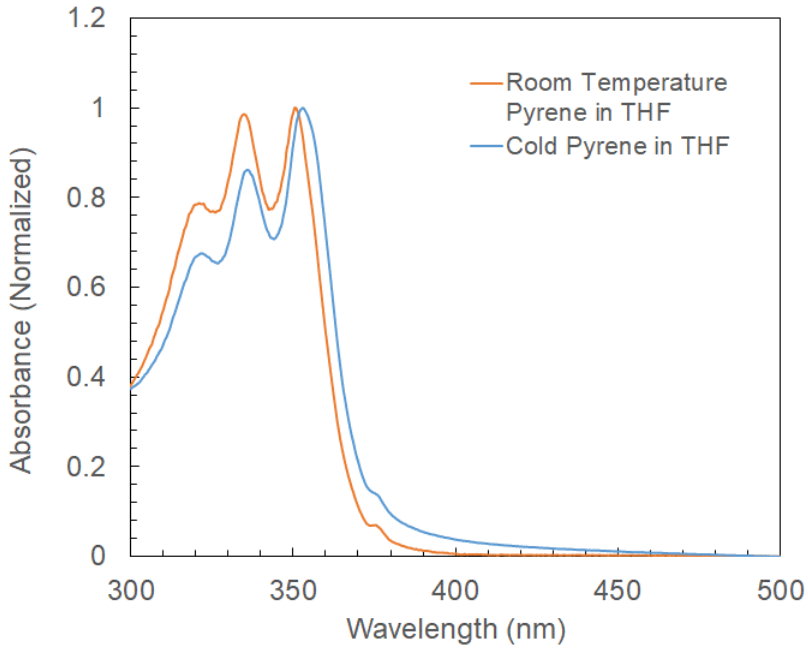

Figure S1.4. Absorption spectra of pyrene nanoparticles prepared as a function of the temperature of the pyrene/THF injection solution. These particular samples were prepared by injecting 0.1 mL of 2 mM pyrene into 10 mL of rapidly stirring 0.1 mg/mL PVA:water, and subsequently storing the nanoparticle suspensions at 5 °C for a period of 2 hrs. Room temperature and cold pyrene in THF refers to the pyrene/THF solution held at 22 and 5 °C, respectively.

The cooled (5 °C) pyrene / THF injection solution showed obvious suppression of bands in the vicinity of the monomer and the most redshifted absorption feature and so we chose to use cooled (5 °C) pyrene / THF injection solution in the preparation of subsequent samples.

Figure S1.5 shows the effect of cooling the aqueous nanoparticle suspensions immediately after their preparation at 5 ^{o}C for various durations of time.

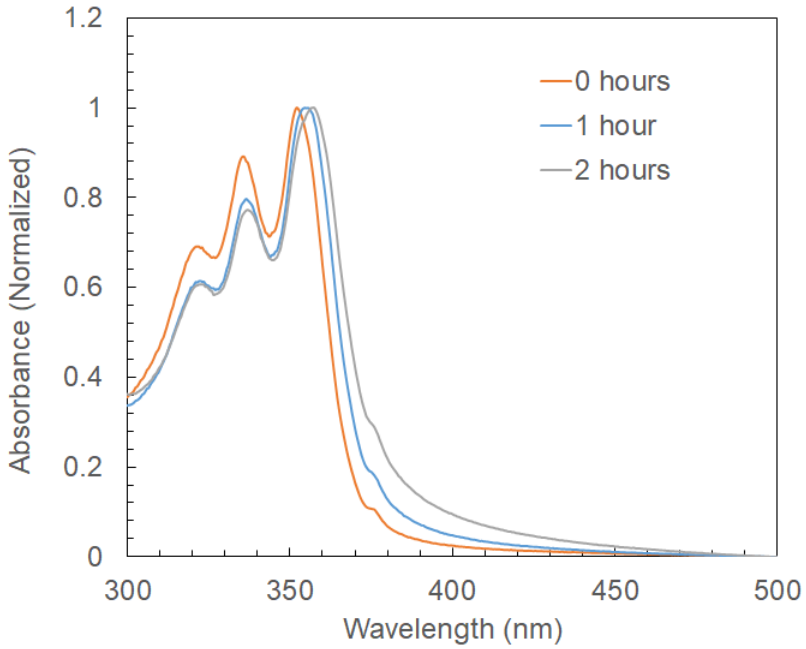

Figure S1.5. Absorption spectra of pyrene nanoparticles prepared as a function of time stored at 5 ^{o}C immediately after their preparation. These particular samples were prepared by injecting 0.1 mL of 2 mM pyrene into 10 mL of rapidly stirring 0.1 mg/mL PVA:water, and subsequently storing the nanoparticle suspensions at 5 ^{o}C for a period of time. The times listed in the figure caption refer to the amount of time the pyrene nanoparticle suspension was stored at 5 ^{o}C before measuring its absorption spectrum.

The aqueous nanoparticle suspension cooled immediately following its preparation at 5 ^{o}C for a period of ca. 2 hr showed the most suppression of bands in the vicinity of the monomer, and the most redshifted absorption feature. On the basis of these results, we chose to cool the aqueous nanoparticle suspension immediately following their preparation at 5 ^{o}C for a period of ca. 2 hr in subsequent sample preparations.

Lastly, **Figure S1.6** shows the reproducibility of the procedure described herein.

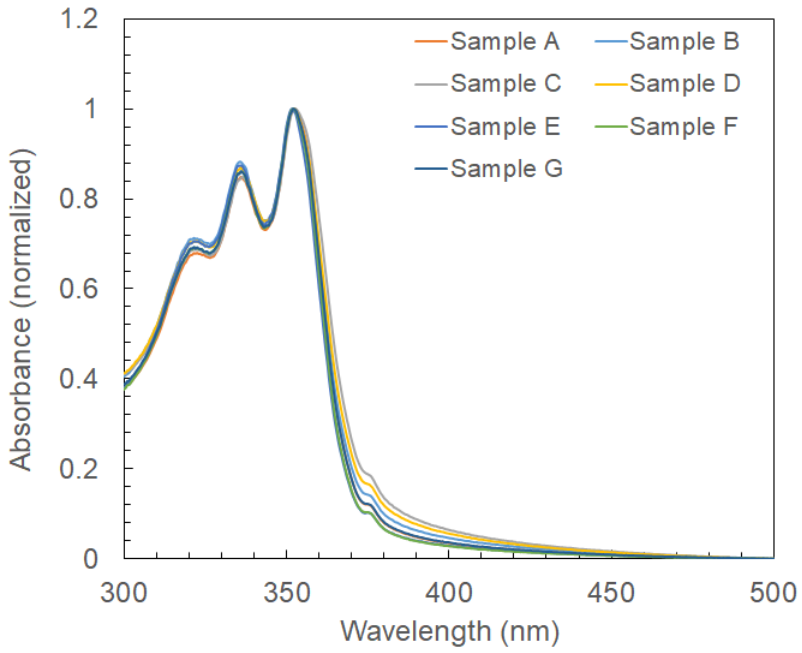

Figure S1.6. Absorption spectra of crystalline pyrene nanoparticles prepared in replicate seven different times. These samples were prepared according to the final procedure developed, i.e., by injecting 0.1 mL of 2 mM pyrene into 10 mL of rapidly stirring 0.1 mg/mL PVA:water, and subsequently storing the nanoparticle suspensions at 5 ^{o}C for a period of 2 hrs. Note that the absorption spectra were obtained on samples that had subsequently warmed to room temperature.

Figure S1.6 shows that the adapted version of the flash precipitation produces nanoparticles comprising primarily strongly coupled pyrene chromophores in a highly reproducible manner.

As a final note, we discuss how the PVA acts to stabilize the nanoparticles. There are several possible ways that the PVA could be acting to stabilize the nanoparticles: (i) the PVA could be coating the surface of the nanoparticles and promote crystallinity within the core, (ii) the PVA could be intercalating into the interior of the nanoparticles and promote crystallinity, or (iii) a combination of coating the surface and intercalation may be responsible for the observed changes. We were unfortunately unable to determine the microscopic origin of how the PVA influences the local molecular packing in the present work.

Section S2: Time-resolved fluorescence of crystalline pyrene nanoparticle suspensions

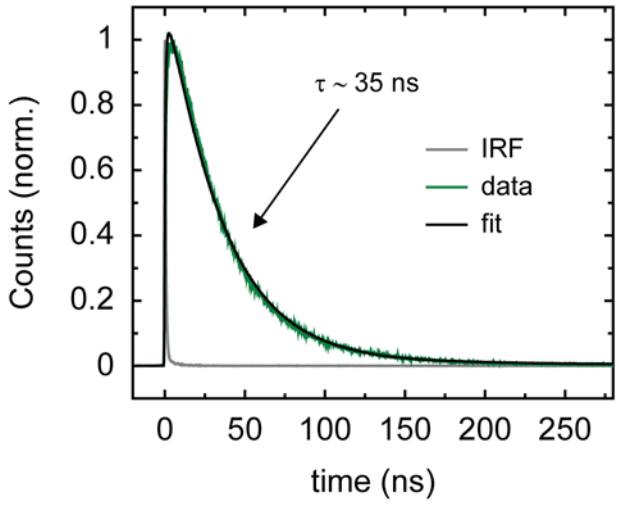

Figure S2. Time-correlated single photon counting measurement of the fluorescence emission of an aqueous suspension of crystalline pyrene nanoparticles. The excitation wavelength for the measurement was 305 nm, and the emission wavelength for the aqueous suspension of crystalline pyrene nanoparticles was 475 nm. The instrument response function had a full-width-at-half-maximum of ca. 0.9 ns. The time constant was derived by convolving the instrument response function with a single-exponential decay function and was found to be ca. 35 ns by determining the best fit to the experimental data.

<u>Section S3</u>: Severe early-time response in femtosecond transient absorption of toluene

In this supporting section, we discuss the origin of the solvent response observed in the transient absorption experiments in toluene and its impact on the results presented in the main text. We first highlight that the primary objectives in performing transient absorption measurements on dilute solutions of pyrene in toluene are: (i) to elucidate the dynamics of the monomer on the timescale of excimer formation in the pyrene nanoparticles, and (ii) to measure a transient absorption spectrum of the monomer in a solvent environment that best approximates that of pyrene in the pyrene nanoparticles.

Figure S3.1 displays the transient absorption of a dilute solution of pyrene in toluene and neat toluene.

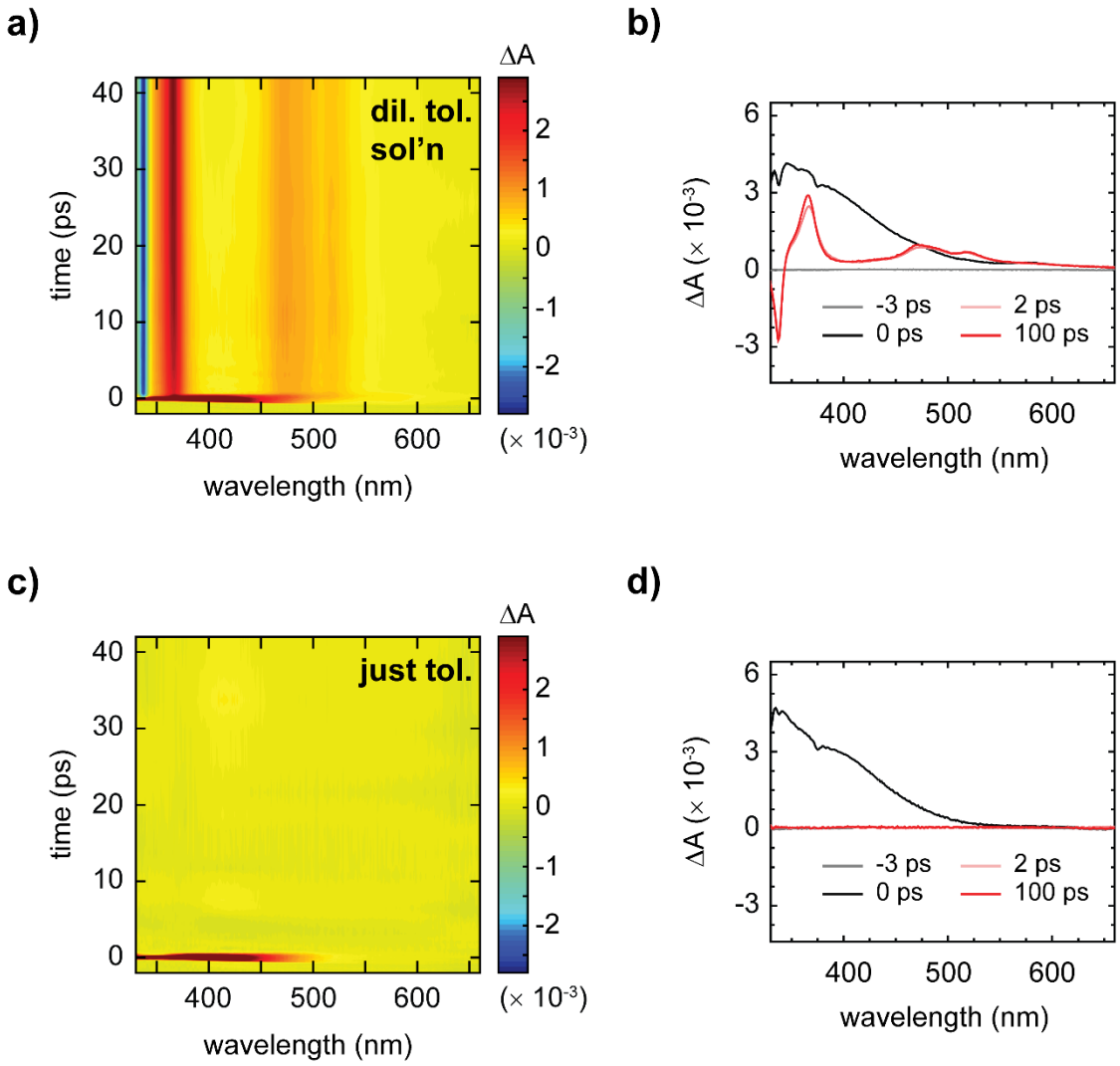

Figure S3.1. Transient visible absorption of pyrene as a dilute toluene solution and of just the solvent toluene. (a and c) Surface plot of transient visible absorption of a dilute solution of pyrene in toluene and of just the solvent toluene. The experiments were performed with the same incident pump wavelength and an incident pump fluence of ca. 335 nm and 200 μJ cm^{-2}, respectively. The scale bar is indicated beside each plot. (b and d) Selected transient spectra for a dilute solution of pyrene in toluene and of just the solvent toluene. Spectra time delays are indicated in the legend. The signal near the time origin of the measurement clearly exhibits a strong, overwhelming solvent response.

A strong, early-time response is apparent in the transient absorption of the dilute solution of pyrene in toluene on the sub-picosecond timescale (**Figure S3.1a**). The magnitude of the response is much larger than that of the transient absorption signals arising from the pyrene monomers (**Figure S3.1b**). Clearly, this early-time response arises from the solvent itself, as the same signal is observed in the transient absorption of neat toluene performed under identical conditions (**Figure S3.1c,d**). Critically, the early-time solvent response does not obscure the pyrene monomer transient absorption spectra measured at 2 and 100 ps as is evident by comparing these spectra with the transient absorption spectra measured in neat toluene on the same timescale (**Figure S3.1b,d**).

We first discuss the origin of the solvent response observed in toluene and why it is so large. The origin of the strong solvent response is likely related to the fact that either: (i) toluene is an aromatic solvent with a large polarizability and so a large nonresonant response can be expected, or (ii) the pump pulse is pre-resonant with toluene's electronic transition at 260 nm.[S2]

We next discuss two ways to mitigate the solvent response observed in toluene. One is to reduce the pathlength of the spectrophotometer cell; on the other hand, it is also possible to simply change the solvent. One good candidate solvent for this purpose is cyclohexane, which being a saturated hydrocarbon has its lowest-energy electronic transition at much shorter wavelength at ca. 160 nm.[S3] Furthermore, cyclohexane is expected to have a lower nonresonant response due to its lower polarizability. **Figure S3.2** displays transient absorption measurements on dilute solutions of pyrene in cyclohexane and on neat cyclohexane.

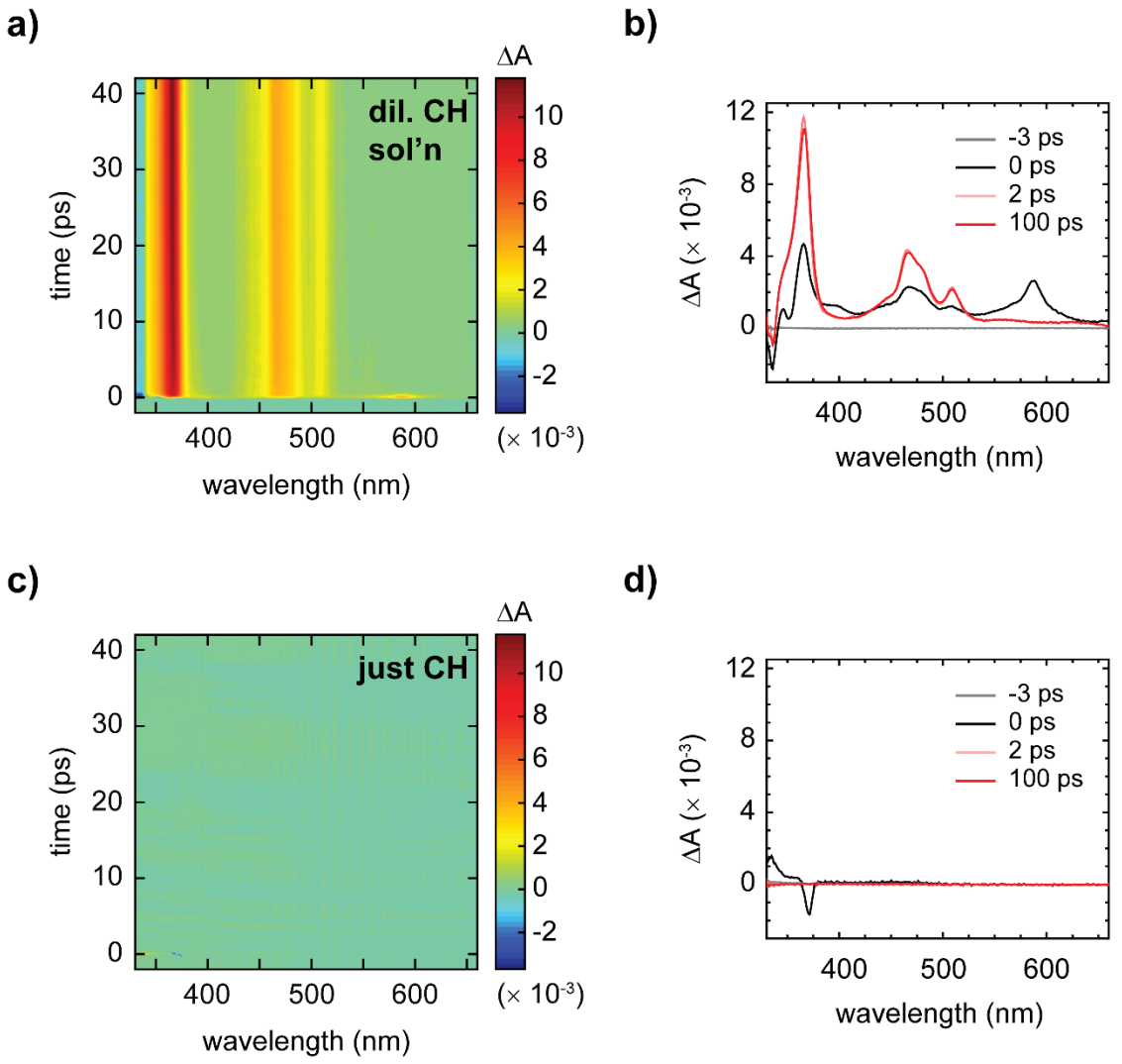

Figure S3.2. Transient visible absorption of pyrene as a dilute cyclohexane solution and of neat cyclohexane. (a and c) Surface plot of transient visible absorption of a dilute solution of pyrene in cyclohexane and of neat cyclohexane. The experiments were performed with the same incident pump wavelength and an incident pump fluence of ca. 335 nm and 50 μJ cm^{-2}, respectively. The scale bar is indicated beside each plot. (b and d) Selected transient spectra for a dilute solution of pyrene in cyclohexane and of neat cyclohexane. Spectra time delays are indicated in the legend. In contrast to the toluene data in the previous figure, the signal near the time origin of the measurement exhibits does not exhibit a large solvent response.

Clearly, very little early-time solvent response is observed in the transient absorption measurements performed in cyclohexane; thus, the early-time solvent response is mitigated through selection of a different solvent. In the transient absorption measurements performed in cyclohexane, we observe the same picosecond-timescale solvation dynamics that we observe in the measurements performed in toluene (see e.g. changes to the 2 and 100 ps transient spectra in

Fig. S3.2b). In addition, we observe dynamics obscured by the early-time solvent response present in measurements performed in toluene (**Fig. S3.2a,b**). Specifically, we observe internal conversion from high-lying singlet excited states (S_n) to the lowest-lying singlet excited state (S_1) on a few hundred femtosecond timescale, consistent with the work of Foggi *et al.*[S4] We should note that this $S_n \rightarrow S_1$ internal conversion step is not observed in transient absorption measurements on the crystalline nanoparticles (see **Figure 4c** of the main text) likely due to the smaller energy gap between the two lowest-lying electronic states in this sample.

Having shown that the early-time solvent response observed in toluene is mitigated in cyclohexane and having shown that the only monomer dynamics masked by the solvent response is an exceptionally rapid (few hundred femtosecond) $S_n \rightarrow S_1$ internal conversion step, we next proceed to discuss the monomer transient absorption spectrum most useful for comparison with the transient absorption of the primary excitons in the crystalline nanoparticles. As described above, one of the primary goals of the measurements was to obtain a spectrum of monomers in dilute organic solvent and compare this spectrum with that of the primary excitons in the nanoparticles. Because the nanoparticles comprise conjugated aromatic molecules, much like toluene, the solvent environment surrounding pyrene molecules in the nanoparticles is much more similar to toluene than cyclohexane. We showed in a prior solvatochromic study that toluene is the solvent that best approximates the solvent environment of conjugated aromatic molecular nanoparticles.[S5]

The effects of solvent environment on the transient absorption spectrum are best evaluated by comparing the data obtained for the monomers in toluene and cyclohexane along with that of the pyrene nanoparticles. **Figure S3.3** displays these transient absorption spectra.

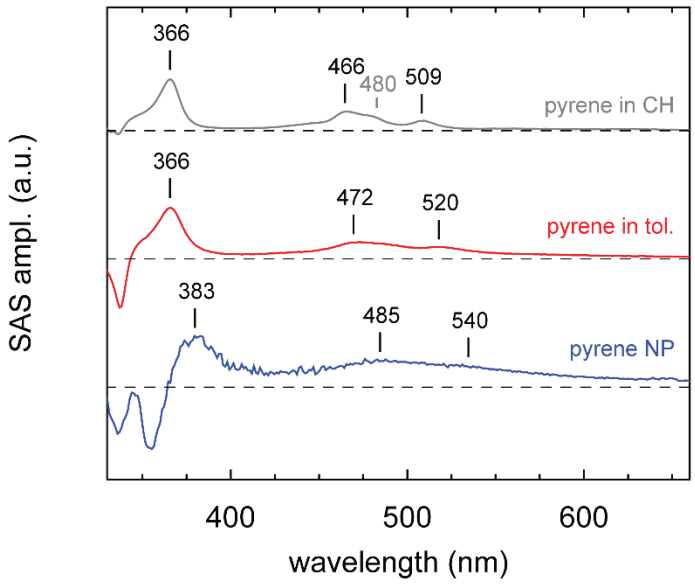

Figure S3.3. Species-associated spectra of primary excitations of pyrene in the form of a dilute cyclohexane solution, a dilute toluene solution, and as crystalline nanoparticles. The species-associated spectra of primary excitations of pyrene in dilute solutions are those obtained after

solvation dynamics. Positions of the most prominent peaks of the different photoinduced absorption bands are indicated.

All of the transient absorption spectra are qualitatively similar. Specifically, ground-state bleaching bands are observed in the vicinity of the $S_0 \rightarrow S_1$ transitions for the different samples. In the case of pyrene in cyclohexane and pyrene in toluene, the ground-state bleach feature peaks at ca. 336 and 338 nm, respectively. In the case of the pyrene nanoparticles, two prominent bleach features peaking at ca. 337 and 354 nm are observed because the ^1L_b electronic transition is excitonically redshifted. Two distinct photoinduced absorption bands additionally appear at longer wavelengths in all datasets. There is a band at short wavelength that peaks at ca. 366 nm for both pyrene in cyclohexane and in toluene; the same band in the pyrene nanoparticles peaks at ca. 383 nm. The latter apparent peak shift likely arises from the overlapping ground-state bleach feature at ca. 354 nm.

Most revealing is a comparison of the photoinduced absorption band appearing in the transient spectrum at the longest wavelengths measured. As reported in the main text, this band is fairly complicated as it has been attributed to multiple overlapping bands arising from multiple electronic transitions present in this spectral window.[S4] Irrespective of this complication, we can still compare the transitions observed for the primary excitations in the different solvents and in the nanoparticles. In all cases, the photoinduced absorption band is qualitatively similar. For pyrene in cyclohexane, the photoinduced absorption band exhibits narrow peaks that are blueshifted with respect to the other datasets. Specifically, peaks are obvious at 466, 480, and 509 nm. For pyrene in toluene, the individual peaks comprising the photoinduced absorption band are broadened. In addition, peaks at 472 and 520 nm are evident, clearly redshifted with respect to the data obtained for pyrene in cyclohexane. We attribute the changes in the band lineshape and peak position observed in the different solvents to solvatochromic effects.[S6] Lastly, in the case of the pyrene nanoparticles, the individual peaks comprising the photoinduced absorption band are further broadened and redshifted with respect to that of both pyrene in cyclohexane and in toluene. Peaks are evident in the nanoparticle sample at 485 and 540 nm. Given the better match between the transient absorption data of pyrene in toluene and the pyrene nanoparticles, we conclude, as we showed previously,[S5] that toluene is best representative of the solvent environment that pyrene molecules experience in the pyrene nanoparticles, which motivated us to compare the transient absorption spectra of the dilute solution of pyrene in toluene with the transient absorption spectrum of primary excitons in the pyrene nanoparticles in the main text.

It is also important to highlight the good agreement between the transient absorption spectra of monomeric pyrene in toluene and primary excitons in the crystalline pyrene nanoparticles, which leads us to further conclude that *primary excitons in the nanoparticles are highly localized*. An additional result in support of this interpretation is that the lowest-energy state (associated with the ^1L_b transition) in crystalline pyrene exhibit signatures of weak electronic coupling (likely as a result of the very small extinction of the transition) which means that, as outlined in the main text, primary excitons in crystalline pyrene are highly localized. This conclusion is expected to be independent of the initial state accessed (i.e., independent of pump wavelength) as a result of Kasha's rule,[S7] which indicates that primary excitations will relax to the lowest-energy state on a rapid timescale; in the case of the monomer, on a timescale of a few hundred femtoseconds and, in the case of the nanoparticles, apparently on a timescale <100 fs.

Section S4: Mathematical justification of two-component kinetic scheme for dilute solution of pyrene in toluene

Figure S4 displays the results of a global target analysis of the transient absorption of the dilute solution of pyrene in toluene modelled according to either single or two-component kinetic schemes. Selected transient kinetics traces, associated fits and residuals, and total rms values are shown.

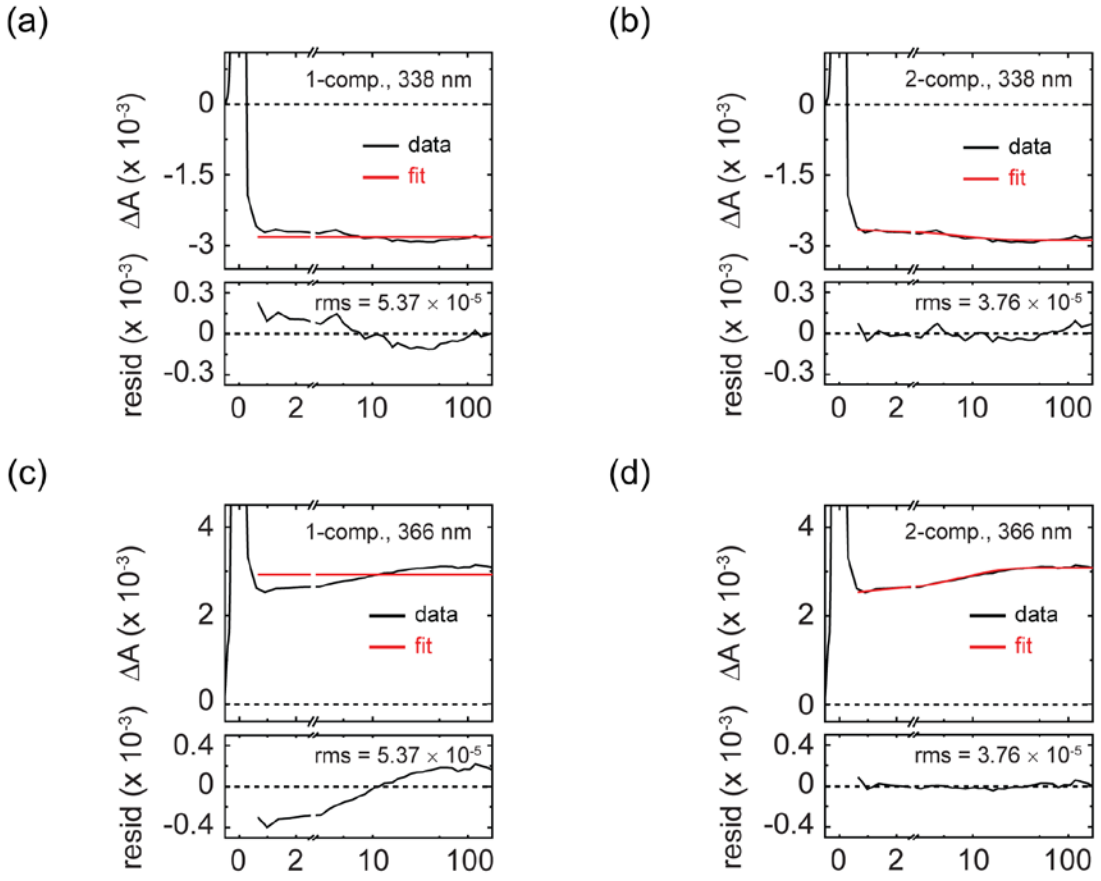

Figure S4. Selected transient kinetics traces for the dilute solution of pyrene in toluene in the vicinity of the origin band of $S_0 \rightarrow S_1$ ground-state bleach and $S_1 \rightarrow S_n$ photoinduced absorption features at 338 and 366 nm, respectively, along with fits, rms values, and residuals from the global and target analysis. (panels a and c) Fits, rms values, and residuals associated with a single component kinetic scheme. (panels b and d) Fits, rms values, and residuals associated with a two-component kinetic scheme.

The lifetimes derived by the single and two-component global target analysis of the transient absorption of the dilute solution of pyrene in toluene are $\tau >> 200$ ps and $\tau_1 = 10$ ps and $\tau_2 >> 200$ ps, respectively. The results of the global target analysis using a single component kinetic scheme clearly do not model the data well, as is reflected by discrepancies between the fit and the data, which in turn results in structure in the residual. The agreement between the data and the fit is

much better for the global target analysis using a two-component kinetic scheme, in which structure is essentially absent in the residuals. The two-component kinetic scheme also significantly improves the rms value associated with the analysis. Clearly two components are justified in the kinetic scheme of the global target analysis of the transient absorption of the dilute solutions of pyrene in toluene.

<u>Section S5</u>: Mathematical justification of three-component kinetic scheme for crystalline pyrene nanoparticle suspensions

We begin by assuming that two components are the minimum necessary to model excimer formation via a global target analysis. That is, transitioning from a primary exciton to an excimer involves a minimum of two components.

Figure S5 displays the results of a global target analysis of the transient absorption of the crystalline pyrene nanoparticle suspensions modelled according to either two- or three-component kinetic schemes. Selected transient kinetics traces, associated fits and residuals, and total rms values are shown.

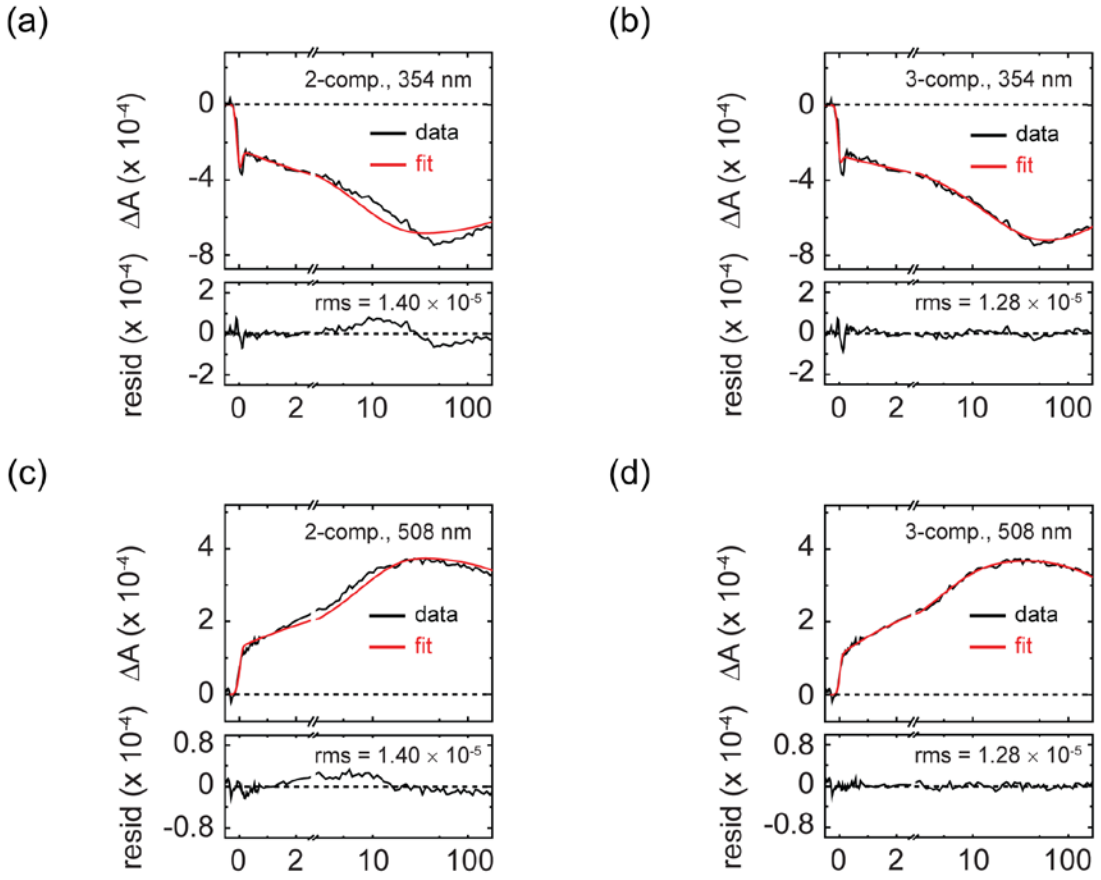

Figure S5. Selected transient kinetics traces for the crystalline pyrene nanoparticle suspensions in the vicinity of the origin band of $S_0 \rightarrow S_1$ ground-state bleach and $S_1 \rightarrow S_n$ photoinduced absorption features at 354 and 508 nm, respectively, along with fits, rms values, and residuals from the global and target analysis. (panels a and c) Fits, rms values, and residuals associated with a two-component kinetic scheme. (panels b and d) Fits, rms values, and residuals associated with a three-component kinetic scheme.

The sets of lifetimes derived by the two- and three-component global target analysis of the transient absorption of the crystalline pyrene nanoparticle suspensions are τ_1 = 7 ps and τ_2 >> 200 ps and τ_1 = 4 ps, τ_2 = 17 ps, and τ_3 >> 200 ps, respectively. The results of the global target analysis using a two-component kinetic scheme clearly do not model the data well, as is reflected by discrepancies between the fit and the data, which in turn results in structure in the residual. The agreement between the data and the fit is much better for the global target analysis using a three-component kinetic scheme, in which structure is essentially absent in the residuals. The three-component kinetic scheme also improves the rms value associated with the analysis. Clearly three components are justified in the kinetic scheme of the global target analysis of the transient absorption of the crystalline pyrene nanoparticles.

Section S6: Evidence against thermal effects on observed changes in transient absorption signals

Given that some excess of energy is deposited into the bath as a result of the energy relaxation that occurs over the course of excimer formation, it is possible that a thermal effect could be invoked to explain the changes in the transient absorption signals that we observe. The observed Stokes shift for the crystalline pyrene excimer, evaluated by taking difference in energy between the peak of the 0-0 band of the lowest-energy crystalline pyrene singlet absorption and the peak of the excimer fluorescence emission, is determined to be ca. 6,000 cm^{-1}. While it is tempting to take this value as the amount of excess energy deposited into the bath following excimer formation, in fact this value reflects the energy relaxation of both excited- and ground-state potential energy surfaces with excimer formation.[S8,9] Warshel and Huler and Cohen *et al.* reported values of ca. 2,800 cm^{-1} and 2,300 cm^{-1}, respectively, for the excess energy of the vertically excited state. This motivates taking a value of 3,000 cm^{-1} as an upper limit for the amount of excess energy available to the system following excimer formation. Taking the value of 3,000 cm^{-1} determined above, and considering that we also need to consider the ca. 1,700 cm^{-1} excess energy provided by the 354 nm excitation light that accesses the second-lowest lying state (accessed through the ^1L_a transition) and not the lowest-energy state (accessed through the ^1L_b transition), we now have a value of ca. 4,700 cm^{-1} for the excess energy in the system immediately following excimer formation.

We next need a means in which to evaluate the temperature of the system according to this amount of excess energy. Fortunately, Foggi *et al.* developed a method in which to estimate the temperature of pyrene molecules as a function of excess energy, which accounts for the discrete vibrational modes of pyrene.[S4] We can therefore take the value determined above and evaluate what is the maximum temperature the pyrene molecules may reach. In this estimation, we consider two limiting cases, one in which a single pyrene molecule bears the majority of the excess energy and another in which both pyrene molecules comprising the excimer bear the excess energy. Considering the temperature of the system in these two limits, we find an excess energy of ca. 460 and 340 K if the energy (and temperature) is distributed over one molecule or over evenly over two molecules, respectively. Considering another limiting case, if we were to excite directly into the lowest-energy state through the ^1L_b transition, these values would be modified to ca. 370 and 270 K, i.e., representing a very modest thermal effect. The values are summarized in **Table S6.1**.

Table S6.1. Molecular Temperatures as a Function of Excess Energy

Pump Wavel. (nm)	Excess Energy (cm^{-1})	One-Molecule Temp. (K)	Two-Molecule Temp. (K)
353	4,700	460	340
376	3,000	370	270

[a] The molecular temperatures were determined according to Foggi *et al. J. Phys. Chem.* **1995**, *99*, 7439–7445.

Figure S6 displays transient absorption data from the crystalline pyrene nanoparticle suspensions excited into the second- and first-lowest lying electronic states, accessed via the ^1L_a and ^1L_b transitions, respectively.

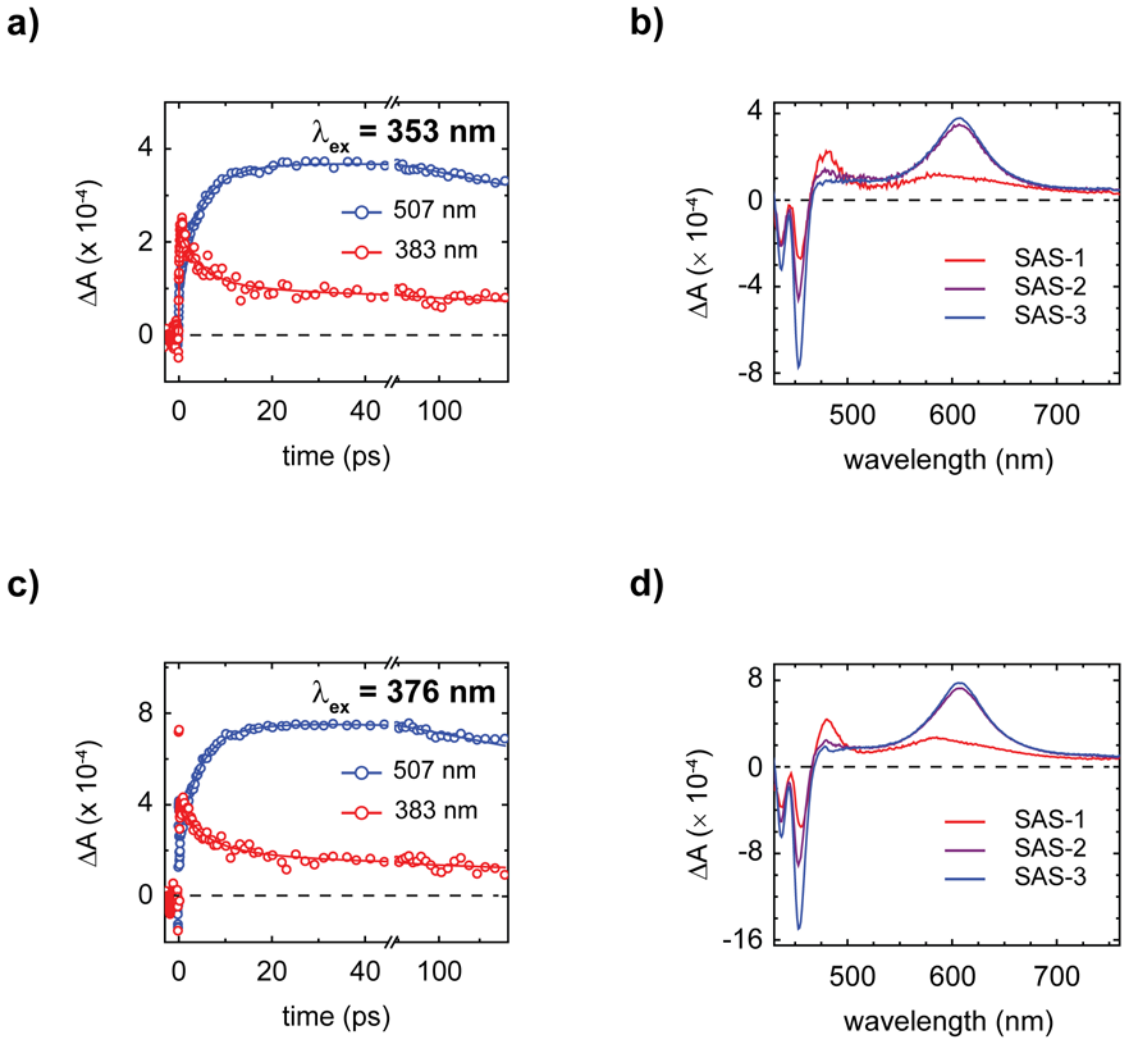

Figure S6. Global target analysis of crystalline pyrene nanoparticle suspensions as a function of excitation wavelength (and excess thermal energy). (a and c) Selected transient kinetics for crystalline pyrene nanoparticle suspensions at pump wavelengths of 353 and 376 nm, respectively. A fit from a global target analysis overlays these transient absorption data. (b and d) Species-associated spectra derived from the global target analysis for crystalline pyrene nanoparticle suspensions at pump wavelengths of 353 and 376 nm, respectively.

The transient absorption kinetics, plotted in panels a and c along with their fits from a three-component global target analysis, are essentially indistinguishable, and essentially the same time

constants are derived for excimer formation at the two different excitation wavelengths (**Table S6.2**).

Table S6.2. Time Constants Determined for Excimer Formation in Crystalline Pyrene Nanoparticles as a Function of Pump Wavelength

Pump Wavel. (nm)	τ_1 (ps)	τ_2 (ps)	τ_3 (ps)
353	4	17	>> 200
376	4	18	>> 200

Critically, the species-associated spectra derived from the global target analysis plotted in panels b and d are also essentially indistinguishable. (The minor deviations observed in the vicinity of the photoinduced absorption band at 383 nm in panel d arise from difficulties in completely eliminating artifacts associated with the 376 nm pump light from these data.) Since there are no changes to either the kinetics of the process or the nature of the spectra by varying excitation wavelength we therefore conclude that excess thermal energy is *not* responsible for the observed changes to the transient spectra. That is, the observed transient absorption signals are independent of pump wavelength (and excess energy).

<u>Section S7:</u> Evidence that near-infrared aromatic 'excimer' bands are derived from single-molecule electronic transitions

In this supporting section, we provide evidence that the near-infrared absorption bands observed for various aromatic 'excimers' (see e.g. refs. S10–S13) are not independent of the electronic structure of the single molecule.

We first consider pyrene. As noted above, near-infrared absorption bands have been observed for various aromatic 'excimers', including pyrene.[S10] The band appears broad and structureless, much like the visible photoinduced absorption band. Central to the thesis of ref. S10 was that single molecule pyrene and other aromatic molecules studied do not have a transition or photoinduced absorption band in the near-infrared spectral region. This implies that the transition is somehow new, as a result of excimer formation, and the authors proposed to consider molecular 'excimers' as a charge-transfer complex with the terminating state of this transition having substantial ion-pair character.

Figure S7.1 displays the electronic absorption spectrum of pyrene in heptane at two concentrations.

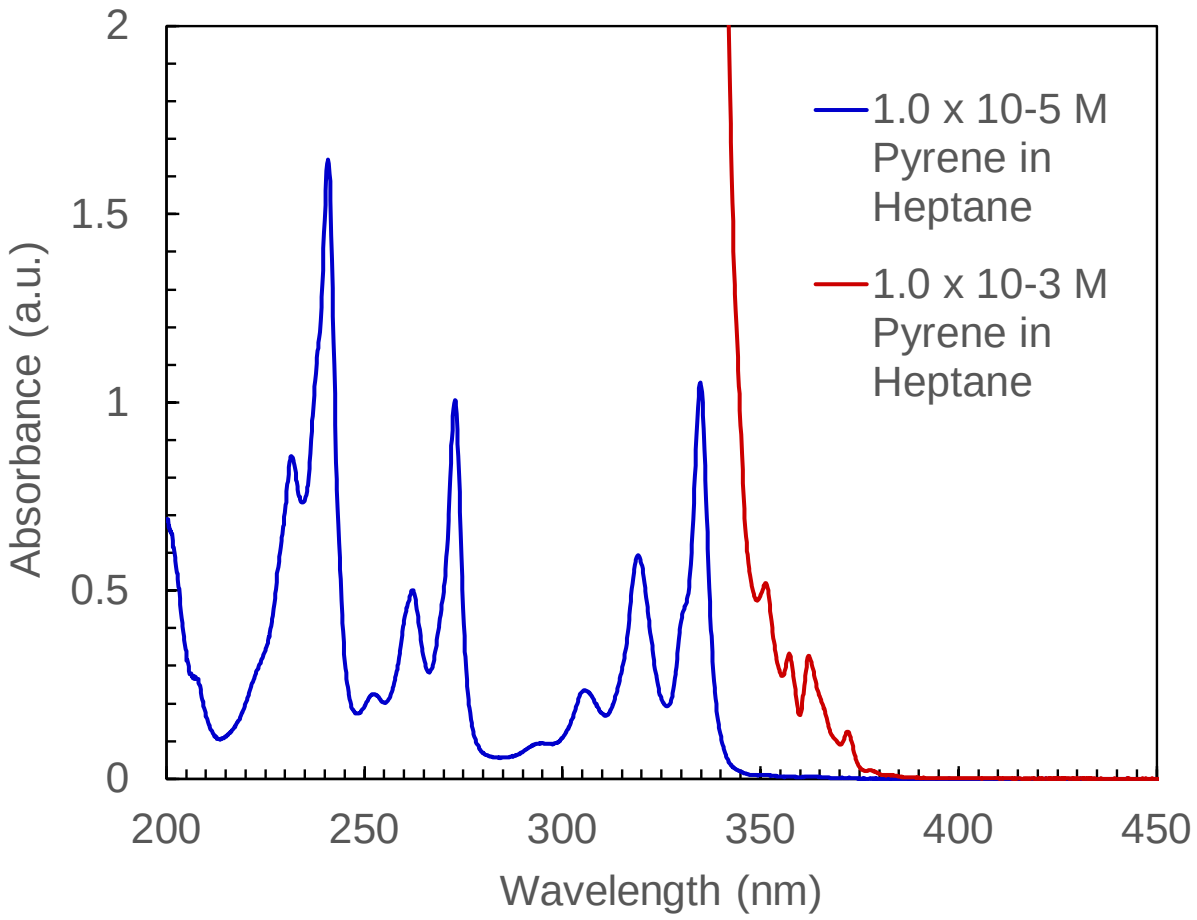

Figure S7.1. The steady-state absorption spectra of pyrene in heptane at two different concentrations. The most concentrated solution measurement was performed to highlight the lowest-energy electronic transition of pyrene, which is only weakly allowed. Four different electronic transitions are apparent in this spectral window spanning from 200 to 450 nm.

As we showed in the main text, the electronic absorption spectrum in toluene is independent of concentration, which we presume to be the case here for pyrene in heptane. Heptane was used because it is a saturated hydrocarbon that does not exhibit electronic transitions in this spectral window, as discussed in some detail in a prior supporting section (i.e. **Section S3**). The absorption spectra measured for pyrene in this spectral range shows the clear presence of four electronic transitions with origin bands at 372, 335, 273, and 241 nm. From the measurement of the origin bands of the four different electronic transitions, we can deduce the energy and peak positions of the three corresponding excited-state electronic transitions, i.e., $S_1 \rightarrow S_n$. Taking the difference between the higher-energy states S_n and the lowest-energy state S_1, we predict three possible $S_1 \rightarrow S_n$ transitions with photoinduced absorption bands peaking at ca. 3300, 1030, and 670 nm. Thus, simply from the electronic absorption spectrum we can expect a photoinduced absorption band for single-molecule pyrene peaking in the near-infrared at ca. 1030 nm. Whether the transition is observed depends on if it has finite oscillator strength, which is not necessarily readily apparent from the steady-state absorption spectrum.

Figure S7.2 displays the transient absorption spectrum of a dilute solution of pyrene in toluene spanning a broad spectral range from ca. 330 to 1600 nm.

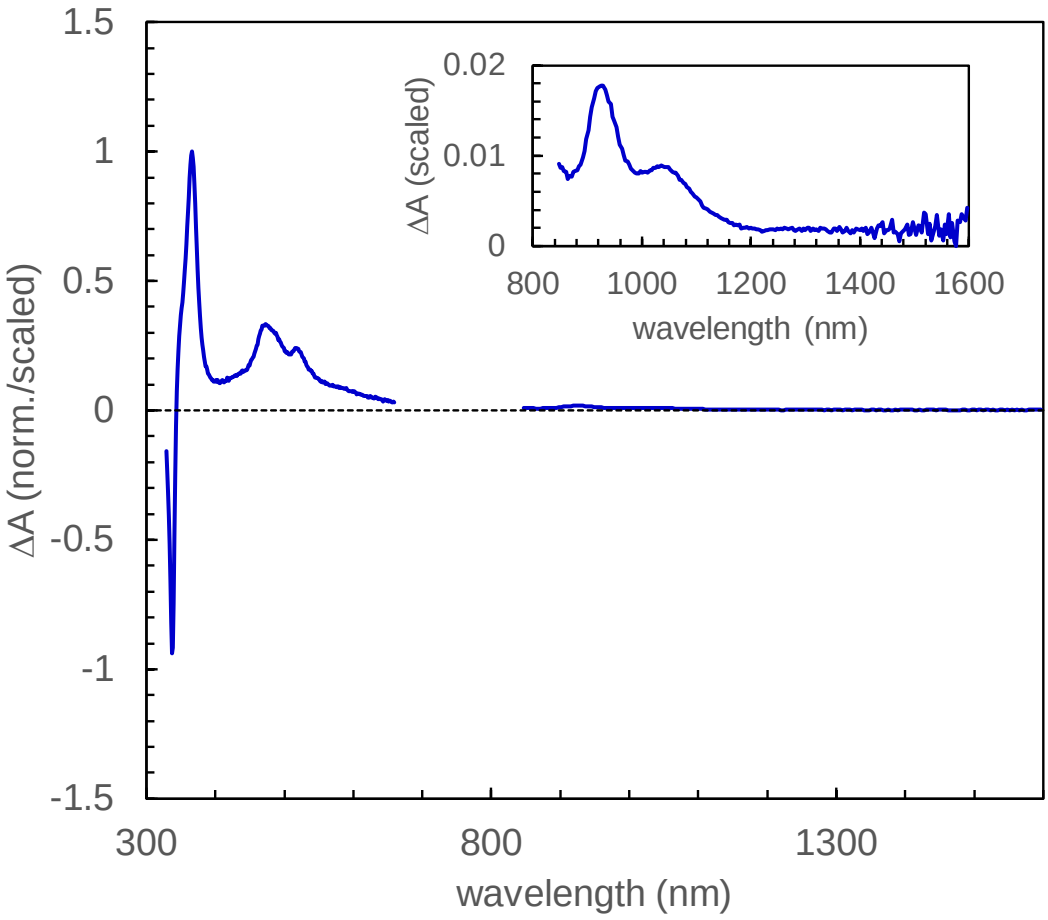

Figure S7.2. Transient absorption of a dilute solution of pyrene in toluene obtained at a time delay of ca. 100 ps. The transient visible and near-infrared absorption spectra were obtained in two different measurements. The same pump wavelength of ca. 335 nm was used for both measurements; the incident pump fluence for the visible and near-infrared measurements was ca. 400 and 800 μJ/cm^2, respectively. We accounted for the different pump fluence in the near-infrared measurement by scaling the signal down, i.e., dividing the signal amplitude by a factor of 2. The inset displays a close-up of the near-infrared photoinduced absorption band scaled in this manner.

As reported in the main text, there are two photoinduced absorption bands in the visible spectral region with the three strongest features peaking at ca. 338, 472, and 520 nm. **Figure S7.2** also shows a much weaker photoinduced absorption band for single molecule pyrene in the near-infrared. As is apparent in the **inset of Figure S7.2**, the origin band of this photoinduced absorption band peaks at ca. 1050 nm. The slight disagreement between this value and that determined above (i.e., 1030 nm) according to the steady-state absorption spectra most certainly arises from a solvatochromic effect. Irrespective of this slight discrepancy, single-molecule pyrene clearly exhibits a transition or photoinduced absorption band in the near-infrared spectral range. The transition is very weak, with its peak extinction at least 50 times less than that of the strongest visible photoinduced absorption band, which may explain why the transition was not considered previously. Having identified this near-infrared photoinduced absorption band for single-molecule

pyrene, we have shown it incorrect to view the terminating state of this transition as being new and somehow independent of the single-molecule electronic structure. Rather, the simultaneous presence of near-infrared single-molecule pyrene and pyrene 'excimer' transitions (the former peaking at ca. 1030 nm in toluene and the latter broadened and redshifted and peaking at ca. 1180 nm according to the measurements of Katoh *et al.*[S10]) fits within our model that the molecular 'excimer' be treated as a singlet exciton, i.e., whose electronic structure is best described according to exciton theory.

We next discuss the generality of this point. For example, we have demonstrated that single-molecule pyrene exhibits a near-infrared transition or photoinduced absorption band, but what of single molecules of other aromatic 'excimers'? For this survey, we consider the three other aromatic 'excimers' studied by Katoh *et al.*, namely 1-methyl-naphthalene, anthracene, and perylene, whose near-infrared excimer photoinduced absorption bands peak at ca. 890, 950, and 1330 nm, respectively.[S10] The electronic transitions of a number of aromatic molecules have been tabulated by Birks,[S14] and we use these values in a similar manner as above to deduce whether or not to expect single-molecule electronic transitions within the vicinity of the respective excimer photoinduced absorption bands. For 1-methyl-naphthalene, the electronic transitions in the steady-state absorption spectra peak at ca. 317, 291, and 224 nm, corresponding to single-molecule $S_1 \rightarrow S_n$ transitions at 3450 and 760 nm. The transition at 760 nm for single-molecule 1-methyl-naphthalene clearly falls within the vicinity of the molecule's excimer photoinduced absorption band that peaks at ca. 890 nm, which is likely strongly redshifted as a result of excitonic effects as was observed above for the pyrene monomer and excimer. Turning to anthracene, two electronic transitions in the steady-state absorption spectra are reported peaking at ca. 374 and 252 nm. The corresponding single-molecule $S_1 \rightarrow S_n$ transition peaks at ca. 770 nm, again in general agreement with the molecule's excimer photoinduced absorption band that peaks at 950 nm.

Lastly, we consider perylene. Perylene exhibits a number of electronic transitions in its steady-state absorption spectrum peaking at 435, 291, 263, 252, 227, and 206 nm.[S14] The corresponding $S_1 \rightarrow S_n$ photoinduced absorption bands peak at ca. 880, 670, 600, 480, and 390 nm. Interestingly, the value for the lowest-energy single-molecule photoinduced absorption band, peaking at ca. 880 nm, is of a much lower wavelength than that observed for the perylene 'excimer' that peaks at ca. 1330 nm. Thus, we have a potential exception. Elegant experimental work by Wasielewski and co-workers, however, has shown that single-molecule perylene indeed exhibits a photoinduced absorption band in the vicinity of the corresponding photoinduced absorption band of the perylene 'excimer'; these authors showed that dilute solutions of single-molecule perylene in toluene exhibit a photoinduced absorption band in the near-infrared with its origin band peaking at ca. 950 nm and identified a weak photoinduced absorption tail extending out to 1600 nm.[S12] It is possible that the terminating state of the transition, or transitions, comprising the tail photoinduced absorption is not so obvious from the steady-state absorption spectrum. Exceedingly weak near-infrared singlet photoinduced absorption bands difficult to identify through the steady-state absorption have recently been reported in elegant work of Grieco *et al.*,[S15] for example. Some additional weight to this argument is evident when considering that Margulies *et al.* recently showed that incorporation of triptycene on one of the nitrogen atoms of the perylene derivative causes a prominent single-molecule near-infrared photoinduced absorption band to appear with an origin band peaking at ca. 1230 nm.[S16]

On the basis of the results and discussion presented above, we conclude that single-molecule transitions or photoinduced absorption bands are generally present in the vicinity of the photoinduced absorption bands of the respective aromatic ‘excimer’ and rule out a depiction of the electronic structure of aromatic ‘excimers’ where the terminating state of the near-infrared photoinduced absorption is considered somehow new and not derived from the single molecule.[S10–13] As we argue in the main text, the electronic structure of aromatic ‘excimers’ is best described according to exciton theory.

<u>Section S8:</u> Derivation of the pyrene 'excimer' diffusion constant in the crystalline pyrene nanoparticles

In this section, we determine the diffusion constant of excimer excitons in the crystalline pyrene nanoparticles.

To determine the diffusion constant, we first need to determine the absolute exciton density associated with the transient absorption signal for each measurement. For the nanoparticle suspensions, this can be accomplished in a relatively straightforward manner by evaluating the number of excitons generated in each nanoparticle and dividing this value by their volume. That is, the exciton density can be expressed as

$$\rho_{exciton} = \frac{N_{exciton}}{V_{NP}}$$

The average number of excitons per nanoparticle can be determined by evaluating the product of the incident pump fluence and nanoparticle cross section.[S17] Thus, the number of excitons is expressed as

$$N_{exciton} = J_{incident} \times \sigma_{NP}$$

In this derivation, we assume as we did in prior work[S5] that the nanoparticle cross section is equivalent to the product of the molecular cross section and number of molecules comprising the nanoparticle, as expressed in the following equation

$$\sigma_{NP} = \sigma_{molec} \times N_{molec}$$

where the number of molecules comprising a single nanoparticle can be expressed as

$$N_{molec} = \frac{V_{NP} \times \rho_{molec} \times N_{Av}}{MW}$$

Thus, the nanoparticle cross section can be expressed as

$$\sigma_{NP} = \frac{\sigma_{molec} \times V_{NP} \times \rho_{molec} \times N_{Av}}{MW}$$

Bringing the above equations together and solving for the exciton density, we have

$$\rho_{exciton} = \frac{J_{incident} \times \sigma_{molec} \times \rho_{molec} \times N_{Av}}{MW}$$

The incident pump fluence, $J_{incident}$, is determined by dividing the measured pump pulse energy by the area of the pump beam estimated via the measured pump spot size. The molar extinction coefficient at 352 nm where the measurements were performed was estimated to be ca. 30,000 M^{-1} cm^{-1}. This estimate is based on the average of the molar extinction coefficient along

the different *a* and *b* projections of the single crystal, which Tanaka measured to be ca. 10,000 and 50,000 M^{-1} cm^{-1}, respectively;[S18] in the crystalline nanoparticle suspensions, the molar extinction will reflect the average of these two values. The molar extinction coefficient can be converted to molecular cross section using Avogadro's number and a unit conversion factor; in this manner, a value of 5×10^{-17} cm^2 was determined. A value of 1.27 g/cm^3 was used to approximate the density of the crystalline pyrene nanoparticles. Lastly, the molecular weight of pyrene is 202.25 g/mol.

With this expression in hand, we arrive at absolute excitation densities corresponding to the transient absorption measurements reported in the main text. We make the additional assumption, given pyrene's unimolecular lifetime of ca. 400 ns and the time constant of ca. 4 ps measured for excimer formation in this work, that all primary excitons are converted into excimer excitons. That is, using the values just mentioned, a simple kinetic analysis[S7] returns an 'excimer' quantum yield of 99.999%. Thus, the exciton densities we calculate for the primary excitons are equivalent to the exciton densities for the excimer excitons.

Figure S8 displays the transient absorption kinetics plotted in the main text **Figure 6** converted to absolute exciton density versus time.

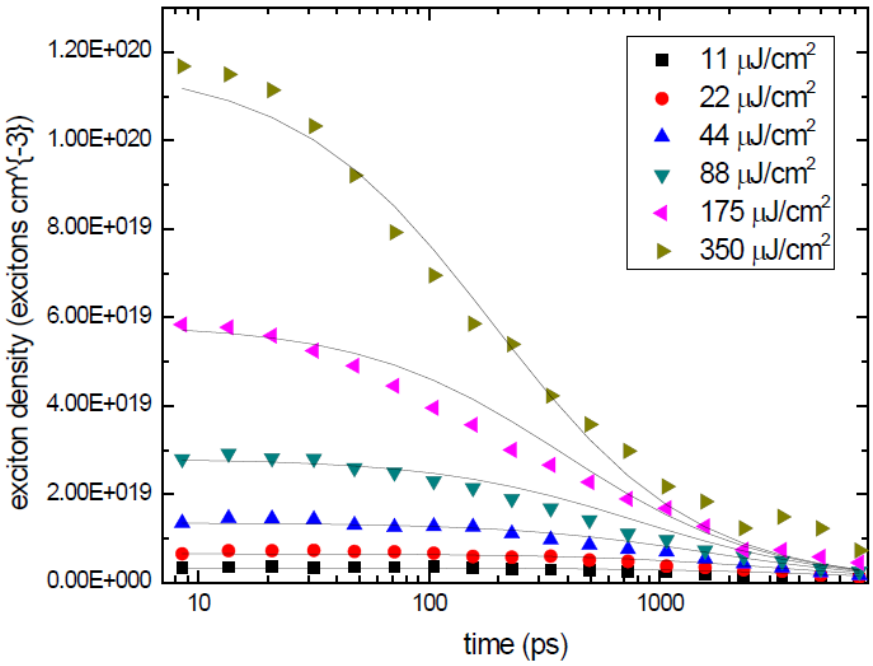

Figure S8. Transient absorption kinetics reported in the main text **Figure 6** converted to absolute exciton density versus time. Measurements performed at six different incident pump fluences are reported. The solid black lines are fits to the data, which was fit globally, according to a solution to the rate equation for bimolecular annihilation that assumes negligible unimolecular decay over the timescale of the measurement. The data were fit on a timescale following excimer relaxation, i.e., several picoseconds and later.

Also overlaying the data in **Figure S8** are fits to the data according to the expression:

$$\frac{1}{[EE]} = \frac{1}{[EE_0]} + \frac{1}{2}k_{bi}t$$

which represents a solution of the rate equation for bimolecular annihilation that, for simplicity, neglects the term that accounts for unimolecular decay.[S19]

The datasets were fit globally according to the expression above. The resulting fits exhibit excellent agreement with the data and give a bimolecular rate constant, i.e., k_{bi}, of 9×10^{-11} cm^3 s^{-1}. The bimolecular rate constant is related to the diffusion constant *D* according to the expression

$$k_{bi} = 8\pi R_C D$$

where R_c is the capture radius which we assume takes on a value of ca. 0.8 nm that corresponds to the center-to-center distance of adjacent pyrene molecular pairs.[S20–22] According to this derivation, and the assumptions made above to arrive at the excitation densities, we estimate a diffusion constant of ca. 5×10^{-5} cm^2 s^{-1} for the crystalline pyrene nanoparticles. This value is identical to that measured by Klöpffer *et al.* using an energy transfer and fluorescence quenching method.[S23]

The observation that the pyrene 'excimers' are mobile indicates that, as we argue in the main text, they exhibit dynamical properties like conventional excitons and so are bested viewed as singlet excitons that have relaxed to an excimer geometry.

Section S9: References

(S1) Pensack, R. D.; Grieco, C.; Purdum, G. E.; Mazza, S. M.; Tilley, A. J.; Ostroumov, E. E.; Seferos, D. S.; Loo, Y.-L.; Asbury, J. B.; Anthony, J. E.; et al. Solution-Processable, Crystalline Material for Quantitative Singlet Fission. *Mater. Horiz.* **2017**, *4*, 915–923.

(S2) Birks, J. B. Excimers. In *Photophysics of Aromatic Molecules*; Wiley-Interscience: London, New York, 1970; pp 301–371.

(S3) Raymonda, J. W.; Simpson, W. T. Experimental and Theoretical Study of Sigma-Bond Electronic Transitions in Alkanes. *J. Chem. Phys.* **1967**, *47*, 430–448.

(S4) Foggi, P.; Pettini, L.; Santa, I.; Righini, R.; Califano, S. Transient Absorption and Vibrational Relaxation Dynamics of the Lowest Excited Singlet State of Pyrene in Solution. *J. Phys. Chem.* **1995**, *99* (19), 7439–7445.

(S5) Pensack, R. D.; Tilley, A. J.; Parkin, S. R.; Lee, T. S.; Payne, M. M.; Gao, D.; Jahnke, A. A.; Oblinsky, D. G.; Li, P.-F.; Anthony, J. E.; et al. Exciton Delocalization Drives Rapid Singlet Fission in Nanoparticles of Acene Derivatives. *J. Am. Chem. Soc.* **2015**, *137*, 6790–6803.

(S6) Reichardt, C. Solvatochromic Dyes as Solvent Polarity Indicators. *Chem. Rev.* **1994**, *94* (8), 2319–2358.

(S7) Turro, N. J.; Scaiano, J. C.; Ramamurthy, V. *Modern Molecular Photochemistry of Organic Molecules*; University Science Books: Sausalito, CA, 2010.

(S8) Cohen, M. D.; Yakhot, V. The Absorption and Fluorescence Properties of Pyrene Crystal: A Theoretical Approach. II. Relaxation Processes. *Chem. Phys.* **1974**, *5*, 27–33.

(S9) Warshel, A.; Huler, E. Theoretical Evaluation of Potential Surfaces, Equilibrium Geometries and Vibronic Transition Intensities of Excimers - Pyrene Crystal Excimer. *Chem. Phys.* **1974**, *6* (3), 463–468.

(S10) Katoh, R.; Katoh, E.; Nakashima, N.; Yuuki, M.; Kotani, M. Near-IR Absorption Spectrum of Aromatic Excimers. *J. Phys. Chem. A* **1997**, *101*, 7725–7728.

(S11) Katoh, R.; Sinha, S.; Murata, S.; Tachiya, M. Origin of the Stabilization Energy of Perylene Excimer as Studied by Fluorescence and Near-IR Transient Absorption Spectroscopy. *J. Photochem. Photobiol. Chem.* **2001**, *145*, 23–34.

(S12) Brown, K. E.; Salamant, W. A.; Shoer, L. E.; Young, R. M.; Wasielewski, M. R. Direct Observation of Ultrafast Excimer Formation in Covalent Perylenediimide Dimers Using Near-Infrared Transient Absorption Spectroscopy. *J. Phys. Chem. Lett.* **2014**, *5*, 2588–2593.

(S13) Son, M.; Park, K. H.; Shao, C.; Würthner, F.; Kim, D. Spectroscopic Demonstration of Exciton Dynamics and Excimer Formation in a Sterically Controlled Perylene Bisimide Dimer Aggregate. *J. Phys. Chem. Lett.* **2014**, *5*, 3601–3607.

(S14) Birks, J. B. *Photophysics of Aromatic Molecules*; Wiley-Interscience: London, New York, 1970.

(S15) Grieco, C.; Kennehan, E. R.; Kim, H.; Pensack, R. D.; Brigeman, A. N.; Rimshaw, A.; Payne, M. M.; Anthony, J. E.; Giebink, N. C.; Scholes, G. D.; et al. Direct Observation of Correlated Triplet Pair Dynamics during Singlet Fission Using Ultrafast Mid-IR Spectroscopy. *J. Phys. Chem. C* **2018**, *122*, 2012–2022.

(S16) Margulies, E. A.; Miller, C. E.; Wu, Y.; Ma, L.; Schatz, G. C.; Young, R. M.; Wasielewski, M. R. Enabling Singlet Fission by Controlling Intramolecular Charge Transfer in π-Stacked Covalent Terrylenediimide Dimers. *Nat. Chem.* **2016**, *8*, 1120–1125.

(S17) Klimov, V. I.; Mikhailovsky, A. A.; McBranch, D. W.; Leatherdale, C. A.; Bawendi, M. G. Quantization of Multiparticle Auger Rates in Semiconductor Quantum Dots. *Science* **2000**, *287*, 1011–1013.
(S18) Tanaka, J. The Electronic Spectra of Pyrene, Chrysene, Azulene, Coronene and Tetracene Crystals. *Bull. Chem. Soc. Jpn.* **1965**, *38*, 86–102.
(S19) Grieco, C.; Doucette, G. S.; Pensack, R. D.; Payne, M. M.; Rimshaw, A.; Scholes, G. D.; Anthony, J. E.; Asbury, J. B. Dynamic Exchange During Triplet Transport in Nanocrystalline TIPS-Pentacene Films. *J. Am. Chem. Soc.* **2016**, *138*, 16069–16080.
(S20) Robertson, J. M.; White, J. G. The Crystal Structure of Pyrene. A Quantitative X-Ray Investigation. *J Chem Soc* **1947**, *0*, 358–368.
(S21) Stevens, B. Some Effects of Molecular Orientation on Fluorescence Emission and Energy Transfer in Crystalline Aromatic Hydrocarbons. *Spectrochim. Acta* **1962**, *18*, 439–448.
(S22) Camerman, A.; Trotter, J. The Crystal and Molecular Structure of Pyrene. *Acta Crystallogr.* **1965**, *18*, 636–643.
(S23) Klöpffer, W.; Bauser, H.; Dolezalek, F.; Naundorf, G. Exciton Diffusion in Pyrene-A Thermally Activated Hopping Process. *Mol Cryst Liq Cryst* **1972**, *16*, 229–245.